Gu *et al. Biochar* (2025) 7:111
https://doi.org/10.1007/s42773-025-00492-w

Biochar

ORIGINAL RESEARCH Open Access

Insight into the crucial role of nano-biochar in the natural formation and bioaccumulation of silver nanoparticles in the rhizosphere by single-particle ICP-MS

Shiguo Gu[1,2], Binbin Sun[2], Fei Wang[2], Wei Zhu[1], Fei Lian[2*] and Jie Li[3]

Abstract

Nano-biochar (nano-BC) is one of the most active fractions in the BC continuum and frequently detected in terrestrial ecosystems. However, a paucity of information exists on reactivity and environmental functions of nano-BC in the rhizosphere. The present study investigated the potential of nano-BC in transforming silver ions (Ag^+) to silver nanoparticles (AgNPs) in the rhizosphere of rice. We found that the synergistic effect of nano-BC and dioxygen secreted from rice roots was essential for Ag^+ reduction to AgNPs. In this process, nano-BC transferred electrons to dioxygen, resulting in the formation of superoxide free radicals, which subsequently donate electrons to Ag^+. Notably, excess nano-BC was unfavorable to dioxygen secretion from roots and thus inhibited the formation of AgNPs. Our results highlight that although nano-BC significantly decreased the uptake of Ag by rice plants, it contributed to the accumulation of AgNPs in plant tissues. TEM and single-particle ICP-MS analyses confirmed the presence of AgNPs not only in intercellular spaces of leaf tissues but also within the interior of leaf cells. These findings indicate that nano-BC plays a critical role in regulating the chemical species and bioaccumulation of redox-active metals (such as Ag) in the rhizosphere, which has important implications for element cycling from the pedosphere to terrestrial vegetation and warrants further investigation.

Highlights

- Nano-BC is an active component in terrestrial ecosystems.
- The synergistic interaction between nano-BC and dissolved oxygen facilitated the formation of AgNPs.
- Nano-BC mediated the rice secretion of O_2 to form O_2-.
- Nano-BC regulated redox-active metal species and bioaccumulation.

Keywords Ag^+, Nano-BC, Rhizosphere, Reduction mechanism, Silver nanoparticle

*Correspondence:
Fei Lian
lianfei2000@126.com
Full list of author information is available at the end of the article

Graphical Abstract

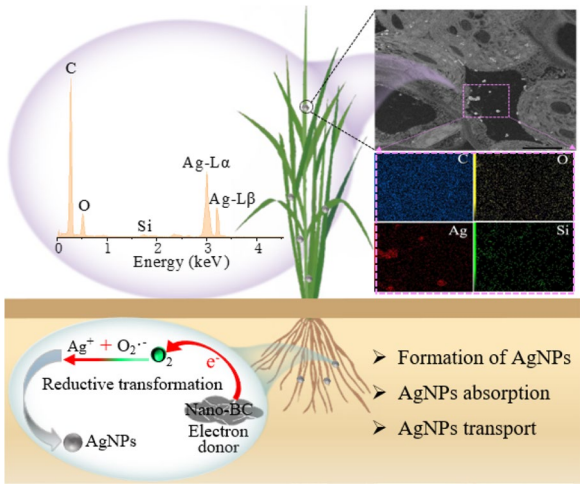

1 Introduction

As a typical transition and precious metal, silver (Ag) and Ag-based materials have been widely used in numerous fields such as consumer goods and medicines due to their superior electroconductibility, ductility, and broad antimicrobial activity (Liu et al. 2023; Nguyen et al. 2024). The extensive production and utilization are inevitable to lead to the release of silver ions (Ag^+) into natural ecosystems. Besides, Ag^+ can also be directly emitted from other Ag contained sources, such as disinfectant products (Rogers et al. 2020), electroplating factory (Vasileiadis et al. 2018), and silver stains (Xiang et al. 2020). It is estimated that the concentration of Ag^+ in the natural water environment is around 1–1000 ng/L (Cymes et al. 2017), even reaching up to 5 mg/L in treated effluents (Zhao et al. 2021; Ge et al. 2022). Due to the relatively low standard oxidation–reduction potential of Ag^+/Ag (0.8 V, 25 °C) (Mwanda and Cuesta 2021), Ag^+ is chemically and biologically active and can be easily reduced by many natural reducing agents and ligands (Akaighe et al. 2011), such as humic acid (Dong et al. 2022), microplastics (Huang et al. 2022), and microorganisms (Boldt et al. 2023). Also, Ag^+ was reported to be photochemically reduced into silver nanoparticles (AgNPs) by soil organic matter under sunlight (Huang et al. 2019). The existing states of Ag remarkably determine its activity, reactivity, and toxicity to organisms. It was shown that AgNPs exhibited a significantly reduced toxicity to human hepatoblastoma cells relative to Ag^+ (Vrček et al. 2016). A previous study found that the uptake rate constants of Ag^+ by wheat roots were 67–87 times higher than those of AgNPs (4.3–5.2 L/(kg·h)) (Dang et al. 2020). These results emphasize that Ag^+ is more mobile, toxic, and bioavailable to plants relative to AgNPs. Therefore, a comprehensive understanding of the transformation of Ag^+ is of importance in predicting and evaluating the fate and ecological effects of Ag.

The species and transformation of Ag in soil are influenced by various factors, including soil composition, pH, organic matter content, and microbial activity. For example, higher content of clay and organic carbon in the soil could enhance the retention of Ag through hetero-aggregation and adsorption (Rahmatpour et al. 2017). Irradiation with sunlight can also promote the reductive conversion of Ag^+ to AgNPs via superoxide radicals (O_2^-) in the aerobic natural surface water (Singh et al. 2019). Similar to metal valence transitions, biochar significantly enhances the photoreduction of Hg (II) to Hg (0) through the generation of O_2^- (Li et al. 2020), while also serving as an electron shuttle to accelerate the bio-reduction of Cr(VI) by O_2^- (Yu et al. 2023). Biochar, a carbon-based material produced through biomass pyrolysis, is ubiquitous in soils. However, its impact on the species and transformation of Ag is less understood, especially in the rhizosphere. Biochar is generally considered an effective soil amendment and widely used in the soil to improve soil fertility and provide other ecological benefits (Yao et al. 2013; Riaz et al. 2017; Liu et al. 2019). Some recent studies have increasingly noticed that nano-biochar (nano-BC) (i.e., BC in the size of < 100 nm) is one of the most active fractions of biochar and plays critical roles in multiple biogeochemical processes including carbon sequestration, elemental

cycling, and transport of contaminants (Zhang et al. 2022; Lian and Xing 2024). Highly mobile nano-BC is likely to be transported from the surface soil into the rhizosphere through infiltration and surface runoff (Xu et al. 2016; Zhang et al. 2022). The introduction of nano-BC might alter the redox states of rhizosphere regions, thus regulating the species and toxicity of Ag to plants (Zhang et al. 2022; Gu et al. 2023). Guo et al. found that wheat root exudates (RE) had high reducing ability to convert Ag^+ to AgNPs under light exposure, facilitated by the formation and redox cycling of photoreactive AgCl (Guo et al. 2019). We previously observed a synergistic effect of nano-BC and rice RE on promoting the phase transformation of ferrihydrite in the rhizosphere (Lian et al. 2022). Considering the geoconductor features of nano-BC (i.e., high electron transfer capacity) (Sun et al. 2017), we hypothesize that nano-BC functions as an electron shuttle, facilitating the continuous transfer of electrons from electron donors to Ag^+ in the rhizosphere.

The major objectives of the present work are to (i) evaluate the ability of nano-BC in transforming Ag^+ to AgNPs in the rice rhizosphere and investigate the related mechanism(s); and (ii) explore the impact of nano-BC on the uptake, distribution, and speciation of Ag in rice plants. The forming kinetics and configuration of AgNPs were examined by a suite of spectroscopic techniques. The secretion of dioxygen and reactive oxygen species (ROS) in the rhizosphere was monitored to elucidate the electron transfer involved in the reduction of Ag^+ to AgNPs. The *in-situ* distribution and speciation of Ag in rice tissues were determined by a combination of single-particle inductively coupled plasma mass spectrometry (ICP-MS) and high-resolution transmission electron microscope (HRTEM). This study provides critical insights into the environmental fate of redox-active metals, the design of nano-BC-based remediation strategies, and the safe deployment of nanomaterials in sustainable agriculture.

2 Materials and methods

2.1 Materials and chemicals

Silver nitrate ($AgNO_3$) (99.8%) was purchased from Sigma-Aldrich. All the other regents with analytical grades or higher were sourced from Solarbio Science & Technology Co., Ltd (Beijing, China). All samples were prepared with ultrapure water (> 18.2 MΩ/cm) and stored in the dark at 4 °C unless stated otherwise. Suspension pH was adjusted using NaOH and HCl. Rice seeds (*Oryza sativa* L., Nan Jing No. 9108) were provided by the Jiangsu Academy of Agricultural Sciences (Nanjing, China).

2.2 Preparation and characterization of nano-BC

Bulk-BC was prepared from sawdust and pig manure by slow pyrolysis, respectively. The tubular reactor containing raw material powders embedded into a muffle furnace was slowly heated (10 °C/min) from room temperature to 550 °C, maintained for 2 h under N_2 atmosphere, and cooled naturally. For preparation of nano-BC, 1.0 g bulk-BC was added into a 150 mL agate jar containing 100 g agate balls (diameter was 6 mm, 3 mm, and 1 mm, respectively), and the mass ratio of biochar to ball was set to 1:100. The agate jars were set into a planetary ball mill machine (TJX-410) and operated at 300 rpm/min for 12 h to produce nano-BC. The obtained samples were labeled as nano-WB (wood biochar) and nano-PMB (pig manure biochar), respectively.

Size and shape of nano-BC were characterized by HRTEM (JEOL, JEM 2100F, Japan). Surface chemical composition was determined using an X-ray photoelectron spectrometer (XPS, Thermo Scientific K-Alpha, USA), Fourier transform infrared spectroscopy (FTIR, Thermo Scientific Nicolet iS5, Thermo, USA), and ^{13}C nuclear magnetic resonance (NMR, Bruker Avance 400, Rheinstetten, Germany), respectively. The detailed procedures were reported in our previous studies (Sun et al. 2020; Sun et al. 2021). For electron paramagnetic resonance (EPR) analysis, 20 mg of solid nano-BC was placed in an EPR tube and analyzed using an EPR spectrometer (Bruker A300, Germany) at 25 °C. The instrument parameters were set as follows: microwave power, 1.92 mW; microwave frequency, 9.85 GHz; modulation amplitude, 1.00 G; receiver, 1.00×10^3; scan width, 200 G; time constant, 10.24 ms; conversion, 30.00 ms; scan time, 30.72 s. The spin intensity was determined by comparing with the 2,2-diphenyl-1-picrylhydrazyl (DPPH) standard. The mediated electrochemical reduction and oxidation capacities of nano-BCs were assessed by electrochemical measurements at room temperature using a CHI610E workstation and a three-electrode cell (Text S1).

2.3 Hydroponic culture and root exudate extraction

Sterilized rice seeds were germinated in vermiculite culture medium with 4% (v/v) NaClO and irrigated with ultrapure water (Yue et al. 2019). The germinated seedlings were irrigated with 25% nutrient solution (pH 5.3) (Table S1) for 14 days. After that, the seedlings were incubated in a growth chamber with a 12-h light cycle, day/night temperature of 25/20 °C, and 60% relative humidity for 60 days. Uniform seedlings were selected and transferred to 6-hole ceramic pots containing 500 mL water for 24 h. The roots of rice seedlings were rinsed three times and the collected water in the pot was immediately filtered with 0.45 μm nitrocellulose membranes to

remove large plant root residues and undissolved substances, and stored at −20 °C as a stock solution of RE. A total organic carbon (TOC) analyzer (TOC-VCPH, Shimadzu, Japan) was used to measure the TOC of RE through high-temperature oxidation, which was detected to be 30.5 mg TOC/L.

2.4 Reduction experiment of Ag^+ in the rhizosphere of rice

Rice seedlings grown for 60 days were transferred into ultrapure water for 24 h to remove the possible interference from other elements in the formation of AgNPs. Then each two seedlings were transplanted into a ceramic jar filled with 500 mL aqueous solution containing suspended nano-BC (5, 10, 20, or 100 mg/L) and 0.5 mM $AgNO_3$ and incubated for 24 h. The measured pH of the aqueous solution was 5.3. To determine the synergistic effects of nano-BC, RE, and rice roots on the reduction of Ag^+ in the rhizosphere, four separate reactive systems were established in ceramic jars: (i) an aqueous solution (500 mL) containing 10 mg/L nano-BC and 0.5 mM $AgNO_3$; (ii) an aqueous solution (500 mL) containing 10 mg/L nano-BC, 0.5 mM $AgNO_3$, and 30.5 mg TOC/L RE; (iii) two rice seedlings were transplanted into an aqueous solution (500 mL) only containing 0.5 mM $AgNO_3$; and (iv) two rice seedlings transplanted into an aqueous solution (500 mL) containing 10 mg/L nano-BC and 0.5 mM $AgNO_3$. To maintain an anaerobic environment, the jars were purged with 200 mL/min N_2 for 60 min and all suspensions were prepared using deoxygenated ultrapure water. Newly secreted O_2 from the root surfaces was monitored every 30 s and lasted for 24 h by microelectrodes, i.e., a micromanipulator with microelectrodes (MM33-2, Unisense) was mounted on a laboratory scaffold (LS18, Unisense), and O_2 was measured at 20 mm from the tip of newly formed roots of uniform length utilizing platinum microelectrode (Rd-N Unisense) (Li and Wang 2012). The detailed procedure and methods were described in our previous study (Gu et al. 2022).

2.5 Free radical determination

The generation of O_2^- during the reduction of Ag^+ was examined by probe molecules. 2,3-bis(2-methoxy-4-nitro-5-sulfophenyl)-2H-tetrazolium-5-carboxanilide (XTT) was selected as the probe molecule for O_2^- quantification. Briefly, 5 mL of 0.05 mM XTT was added to the reaction solution obtained from Ag^+ reduction in various systems, and the XTT formazan concentration in the filtered supernatant was quantified spectrophotometrically at 475 nm, with the detailed methodology presented in Text S2. To clarify the critical role of O_2^- in the reduction of Ag^+, a quenching experiment was conducted by adding superoxide dismutase (SOD, 150 U/mL) as a typical scavenger for O_2^- to the reaction system (iv), i.e., rice seedlings + nano-BC + $AgNO_3$ before the measurement of AgNP formation.

2.6 Measurement and characterization of formed AgNPs

UV–visible spectroscopy (UV-1800, Shimadzu, Japan) was used to monitor the formation of AgNPs in the aqueous solution. Concentrations of total Ag in solutions were determined using ICP-MS (ICAP-TQ, Thermo) by cloud point extraction (CPE) method as described in Text S3. Single-particle ICP-MS (SP-ICP-MS) was carried out by the same ICP-MS instrument and Syngistix Nano-Application module in single-particle mode to determine the formation and concentration of AgNPs (Schwertfeger et al. 2017). Briefly, the aqueous solutions sampled from different treatments were ultrasonicated (600 W) for 30 min, followed by centrifugated at 6000 g for 20 min to separate the formed AgNPs. Then, the supernatant was filtered through a 0.22 μm nylon syringe filter (Millex Millipore) and diluted 50 times using ultrapure water for SP-ICP-MS analysis (Schwertfeger et al. 2017). Crystal structure and chemical information of the formed AgNPs were examined by HRTEM coupled with selected area electron diffraction (SAED). Energy dispersive spectroscopy (EDS) analysis was performed to examine the relative abundance of AgNPs. To quantitively evaluate the impacts of different nano-BC on the reduction efficiency of Ag^+ in the rhizosphere of rice, reduction kinetics of Ag^+ was conducted in the reaction system (iv) containing nano-WB and nano-PMB, respectively. The aqueous solution was sampled at 0.5, 1, 3, 5, 7, 9, 12, 15, and 18 h during reactions, and the formation of AgNPs was detected by SP-ICP-MS. The reduction kinetics was described by a pseudo-first-order kinetic equation (Adegboyega et al. 2012), as calculated using Eq. 1.

$$-\mathrm{Ln}(C_0/C_t) = \mathrm{K} * t \quad (1)$$

where C_0 and C_t are the concentrations of AgNPs at time beginning and time t, respectively; k is the pseudo-first-order rate constant.

2.7 Determination of Ag content and microscopic observation of AgNPs in rice leaves

To further determine the possible translocation of formed AgNPs from roots to aboveground tissues of rice plants, the rice roots and shoots treated by nano-WB (10 mg/L) were harvested, oven-dried, and then separately pulverized into fine powders. The fine powders (50 mg) were digested in a microwave accelerated reaction system (CEM Corp.) at 190 °C for 30 min using a 1:1 mixture of HNO_3 (3 mL) and ultrapure water. The digested solution was filtered through a 0.22 μm membrane for the analysis of Ag and AgNPs by ICP-MS and SP-ICP-MS,

respectively. Transverse sections of the leaf and root segments were prepared using a diamond knife (Diamond Ultra 45°, Diamond, Germany) on an ultramicrotome (Leica UC7, Leica, Germany). The resin blocks were subsequently loaded onto a copper mesh and installed onto the TEM (Hitachi, HT7800, Japan) sample stage. Scanning TEM (STEM) observation was performed on rice tissue sections using bright field and high-angle annular dark field (HAADF) modes. Rice tissue sections were monitored using TEM with EDS elemental mapping in the bright field mode.

2.8 Statistical analysis

All experiments were conducted four replicates, and the results were presented as the means ± standard deviation. Differences between treatments ($p < 0.05$) were analyzed by one-way analysis of variance (ANOVA) using the Duncan test. All data analyses were conducted using IBM's SPSS Statistics version 26.0 (USA).

3 Results and discussion

3.1 Structural properties of nano-BC

TEM images indicate that nano-WB and nano-PMB were in the forms of nanosized spherical structure (Fig. S2), and their average sizes were in the ranges of 61.47 ± 4.35 and 69.22 ± 5.36 nm, respectively (Fig. S3). XPS analysis revealed that nano-WB had higher contents of C and O than nano-PMB, while nano-PMB had higher contents of Si and Ca (Table S3). The higher mineral content of nano-PMB could be explained by the fact that manure-derived biochar is generally rich in minerals (Qiu et al. 2023), which has a profound influence on the chemical activity of nano-BC. As shown in Fig. S1A, the content of C=C/C–C in nano-PMB (35.17%) was higher than that in nano-WB (30.27%), indicating a higher content of sp^2- and sp^3-hybridized carbons in nano-PMB. Comparatively, nano-WB had a higher percentage of oxygen-containing groups, including –OH (40.96%) and C=O (28.77%), than nano-PMB (–OH: 43.34%, C=O: 21.29%). Some typical functional groups such as –OH at 3404 cm^{-1}, aromatic C=C and/or C=O stretching between 1626 and 1421 cm^{-1}, C–O at 1097 cm^{-1}, and aromatic C–H at 877 cm^{-1} on the surfaces of nano-BC were also revealed by FTIR (Fig. S1B). The chemical structure of nano-BC was further characterized by solid ^{13}C NMR, and the results are shown in Fig. S1C. Two typically broad bands at approximately 135 and 35 ppm could be assigned to sp^2- and sp^3-hybridized carbons, respectively. The surface band assignments were as follows: the peak near 135 ppm represented aromatic carbon, rotating CH_3 groups and $(CH_2)_n$ segments resonated at 30 ppm, and C=O functional groups located between 200 and 230 ppm (Qu et al. 2016; Mao et al. 2010). The

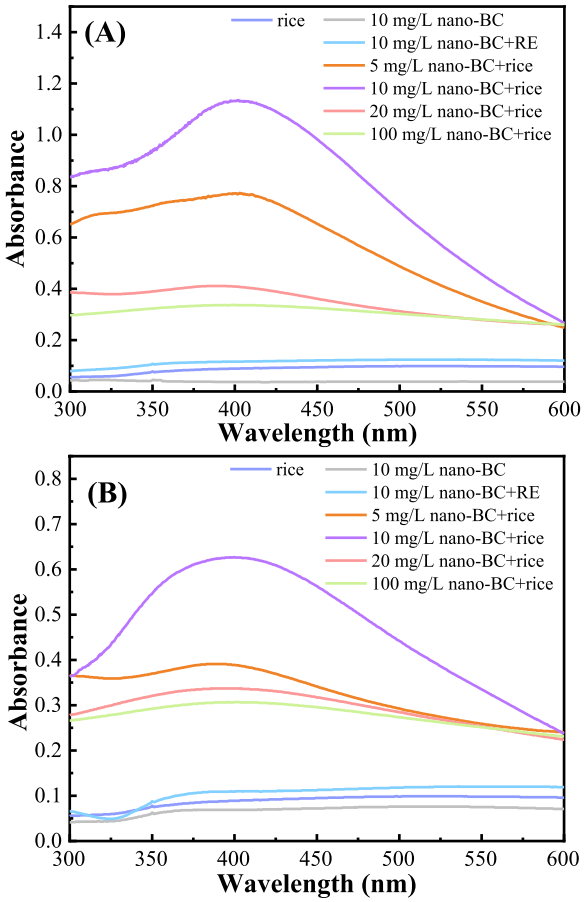

Fig. 1 Determination of AgNP formation using UV–vis in the presence of (**a**) nano-WB and (**b**) nano-PMB with different concentrations

^{13}C NMR results revealed that the intensity of functional group peaks in nano-WB was higher than that of nano-PMB. The oxygen content of nano-WB was 14.46% higher than that of nano-PMB (3.21%), and the (O + N)/C ratio in nano-WB was 0.32, higher than that of nano-PMB (0.28), signifying that nano-WB had a relatively higher polarity (Table S2). The absolute ζ potential values of nano-WB were all higher than those of nano-PMB as a function of pH, probably owing to its higher content of oxygen-containing groups (Fig. S1D). At pH 5.6, the ζ potential of nano-WB was approximately −27.5 mV, much lower than that of nano-PMB (−20.8 mV), signifying its more negatively charged surfaces and higher dispersibility in the aqueous solution.

3.2 Nano-BC induced formation of AgNPs in the rhizosphere

UV–Vis spectra collected from the aqueous reaction systems elucidated the formation of AgNPs, as illustrated in Fig. 1. It has been demonstrated that the UV–Vis

characteristic peak of spherical AgNPs generally appears at 410 nm (Hou et al. 2013; Zhang et al. 2016). The formation of AgNPs was only observed in the system iv (rice plants + nano-BC + $AgNO_3$), where the content of AgNPs significantly increased with the dosage of nano-BC and peaked at 10 mg/L, reflected by the gradually enhanced absorbance in the UV–Vis (Fig. 1). It is worth noting that no absorbance peak was observed in the combination of nano-BC + $AgNO_3$ + extracted RE (i.e., system ii). The results demonstrate the little impact of RE on the formation of AgNPs and highlight the critical role of living roots—rather than RE—in the nano-BC induced formation of AgNPs in the rhizosphere of rice plants. The decreased content of AgNPs with further enhanced nano-BC dosage (> 10 mg/L) suggests that excessive nano-BC was unfavorable to the electron transfer from potential electron donors to Ag^+ in the rhizosphere. We previously found that excess nano-BC attached to rice roots inhibited the dioxygen secretion by blocking aerenchyma and negatively affected the metabolism of rice plants (Gu et al. 2022). It was reported that aeration with O_2 in biochar-ascorbic acid systems accelerated the electron transfer from persistent free radicals (PFRs) in biochar to dioxygen forming O_2^-, which improved the degradation of bisphenol A (up to 69.4%) (Zhu et al. 2024). Thus, the concentration of secreted O_2 from root surfaces within 24 h was measured before and after binding with nano-BC. The highest value of O_2 concentration appeared when the dosage of nano-BC reached 10 mg/L (Fig. S4-S5). However, at higher concentrations of nano-BC, the secreted O_2 levels gradually declined, which was highly consistent with the trend of Ag^+ reduction. The results indicate that secreted O_2 from rice roots played a crucial role in the formation of AgNPs (see more discussion below).

3.3 Unique properties of newly formed AgNPs in the rhizosphere

The features of AgNPs formed in the rhizosphere treated by 10 mg/L nano-BC were characterized using TEM, HRTEM, EDS, and SAED, respectively, as depicted in Fig. 2. TEM images indicated that the generated AgNPs exhibited a near-spherical shape with an average size of 37.6 ± 2.19 nm (Fig. 2a), and they were mainly composed of three crystal faces, including {220}, {200}, and {111}, with lattice spacings of d = 0.145 nm, d = 0.205 nm, and d = 0.236 nm (Fig. 2b), respectively, consistent with the characteristic pattern of metallic Ag (Jiang et al. 2016). EDS analysis revealed that the observed nanoparticles were mainly composed of Ag (Fig. 2c). The gradually yellowing color of the suspensions in different treatments also indicates the formation of AgNPs (Fig. S6) (Huang et al. 2019). The SEAD analysis (Fig. 2d) identified the characteristic patterns related to the atomic planes of three crystal faces ({220}, {200}, and {111}) of AgNPs (Yang et al. 2017). These characterization results demonstrate that the presence of nano-BC facilitated the reduction of Ag^+ to AgNPs in the rice rhizosphere. Furthermore, these data suggest that the hotspot effect of rhizosphere might be strengthened by the introduction of nano-BC, and thus more effort should be paid to explore the catalytic role of nano-BC in the rhizosphere.

3.4 Formation kinetics of AgNPs

The reduction kinetics of Ag^+ to AgNPs in different treatments was investigated and only the combination of rice roots, nano-BC, and $AgNO_3$ witnessed a rapid formation of AgNPs with increasing reaction time (Fig. 3a). The formation kinetics of AgNPs was well fitted by a pseudo-first-order kinetic equation (Adegboyega et al. 2012) and the rate constant (k) mediated by nano-WB was 0.095 h^{-1} ($R^2 = 0.979$), while that was 0.032 h^{-1} mediated by nano-PMB ($R^2 = 0.976$), almost three times lower than that of nano-WB. Comparatively, the reduction rate constant (k) of Ag^+ mediated by particulate organic matter, graphene oxide, and natural organic matter was reported to be 0.00249 h^{-1} (Huang et al. 2019), 0.0012 h^{-1} (Wang et al. 2015), and 0.000175 h^{-1} (Hou et al. 2013), respectively, which reflected the extraordinary catalytic capacity of nano-BC in the rhizosphere of rice. The higher rate constant of nano-WB relative to nano-PMB could be ascribed to their distinct physicochemical properties, which will be discussed in the following sections. Particle sizes of the formed AgNPs measured by SP-ICP-MS were approximately centered at 37.58 ± 3.26 nm and 41.28 ± 3.20 nm in the treatments of nano-WB and nano-PMB, respectively (Fig. 3c, d). These ultrafine AgNPs were incline to attach to the root surfaces (Torrent et al. 2022; Larue et al. 2014), thereby enhancing the chances to be taken up by rice roots. It was observed that AgNPs with particle sizes less than 75 nm could be directly absorbed and accumulated by lettuce roots (Torrent et al. 2022). Similar results were reported for smaller-sized AgNPs (e.g., 38.6 nm and 56 nm) in different plants (e.g., lettuce (Larue et al. 2014) and tobacco (Peharec Štefanić et al. 2021)), indicative of the high possibility of AgNPs formed in this study to be taken up directly by rice roots.

3.5 In situ distribution and speciation of AgNPs in rice tissues

The impact of nano-BC on the uptake and accumulation of Ag by rice plants was examined, with nano-WB selected as a representative of nano-BC due to its more prominent effect on the formation of AgNPs as mentioned above. Total Ag contents in the roots and shoots of rice plants were measured and it was evident that Ag

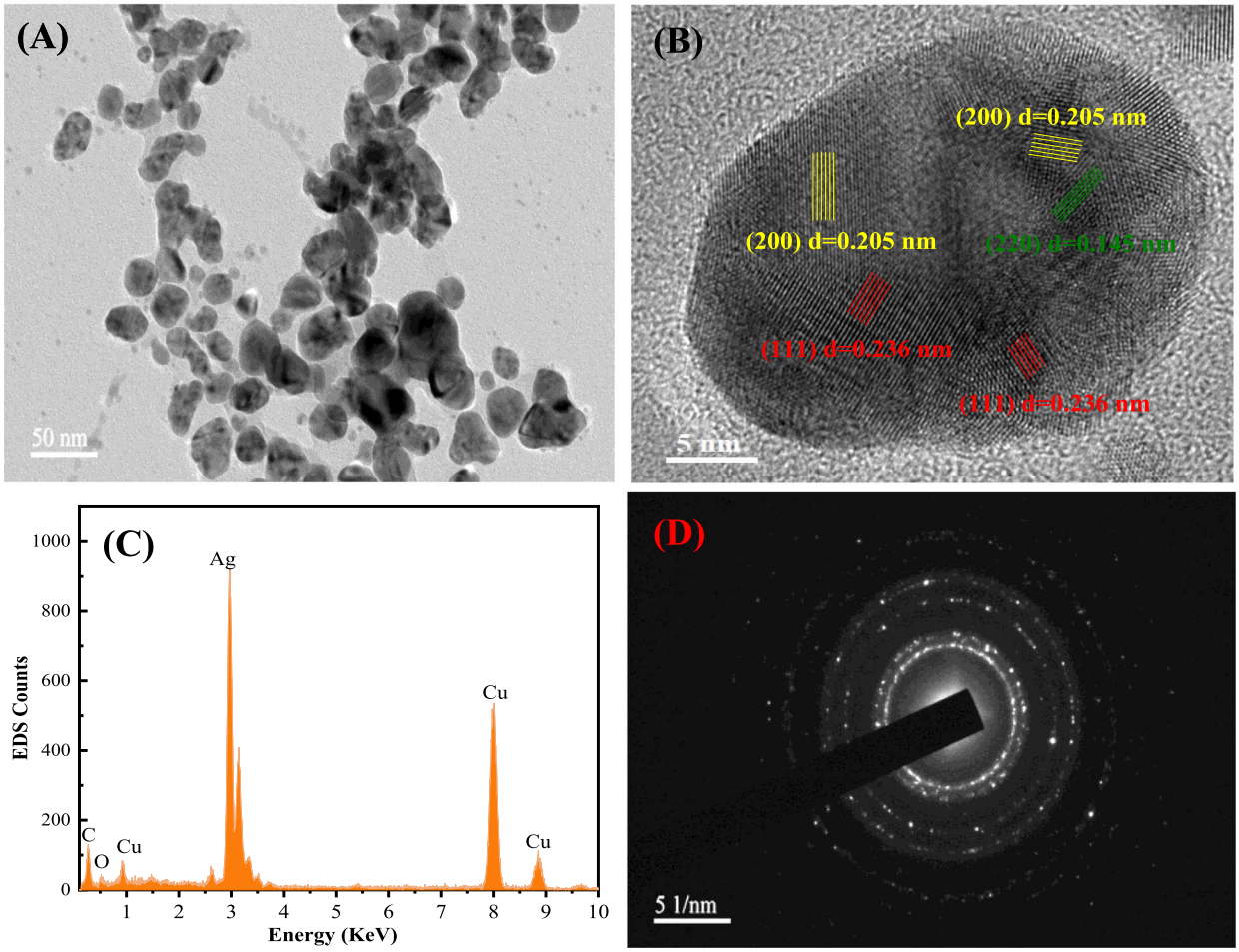

Fig. 2 Identification and characterization of generated AgNPs via the reduction of Ag^+ (0.5 mM) by 10 mg/L nano-WB in the rice rhizosphere. TEM (**a**), HRTEM (**b**), EDS (**c**), and SAED (**d**)

content in the roots and shoots treated with nano-BC was significantly ($p < 0.05$) lower than that of control (Fig. 4a). The results are consistent with many previous studies that charred materials including colloidal-BC have a great potential in sequestrating heavy metals in soils owing to their high sorption affinity to metals (Li et al. 2021; Islam et al. 2022). Different from many observations in the literature, however, we noted that as high as 2.89 mg/g of AgNPs was identified in the rice roots treated by nano-WB and no AgNPs can be observed in the $AgNO_3$ control (without nano-BC) based on the SP-ICP-MS results (Fig. 4b). This indicate that the newly formed AgNPs in the rhizosphere could be taken up and accumulated in the rice roots. Moreover, a measurable content (0.01 mg/g) of AgNPs was observed in the rice shoots for the nano-BC treatment. It can be calculated that 48.05% and 33.33% of Ag accumulated in the shoots, respectively, were present as AgNPs, owing to the presence of nano-BC in the rhizosphere. These observations indicate that nano-BC not only inhibits the uptake of heavy metals by plants but also remarkably regulates their species in the tissues of plants, which has profound implications for elemental biogeochemical process and food security of human beings. To further validate the uptake and accumulation of AgNPs by the rice plants, both TEM imaging and EDS analysis were conducted. High-electron-density dark aggregates were identified not only in the intercellular spaces of root tissues (Fig. S7a, b) but also in various cellular compartments, including chloroplasts, cell walls, membrane-bound structures like vacuoles (Fig. 4c, d). STEM/HAADF images (Fig. 4e, f) revealed that the sizes of individual particles within the bright aggregates were around 40 nm, consistent with the particle size of AgNPs observed by TEM (Fig. S7d). Furthermore, the corresponding EDS spectra (Fig. 4g and S8) clearly exhibited the characteristic peaks of Lα and Lβ spectral lines for silver at 3 keV and 3.18 keV, respectively, aligning with the results reported

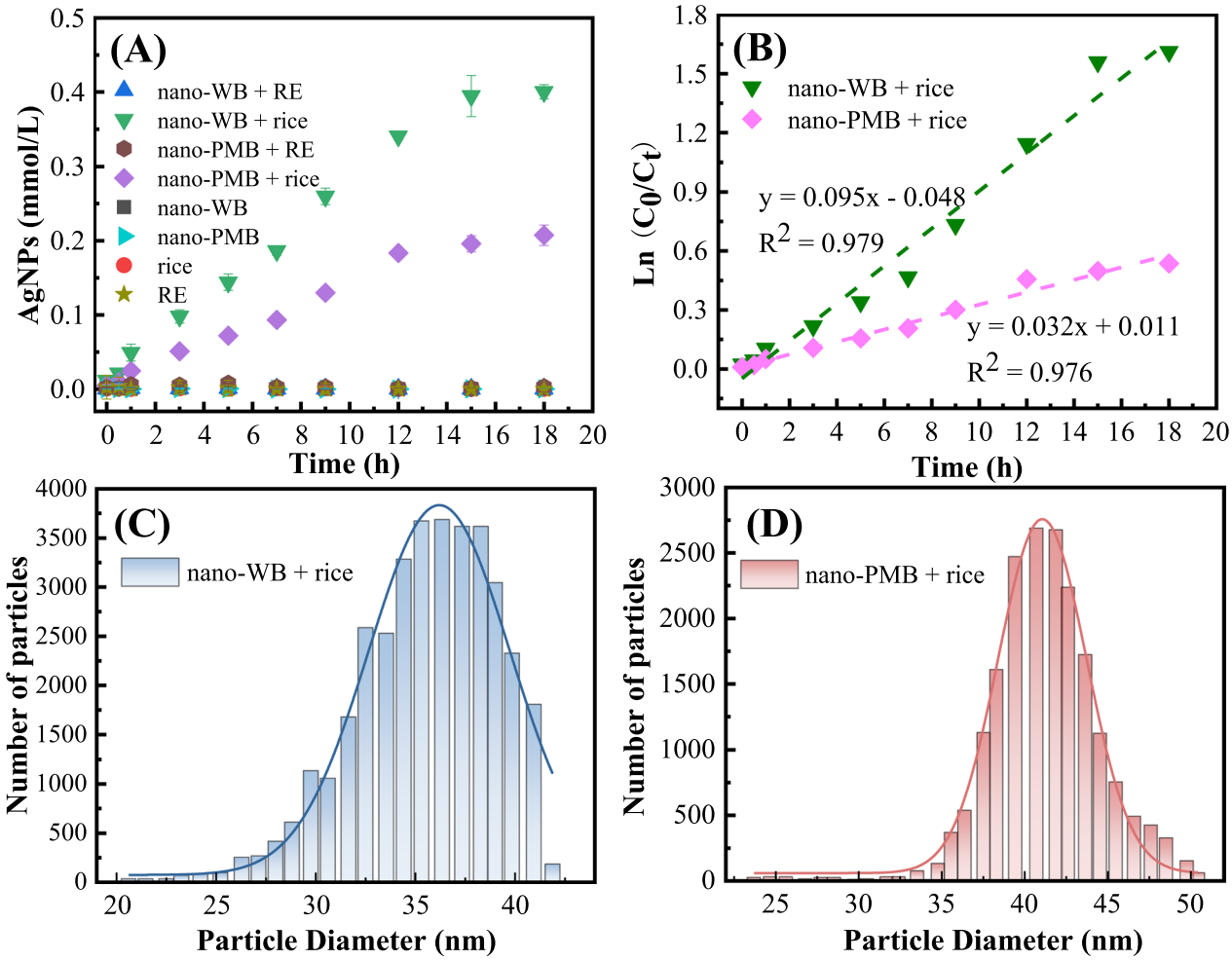

Fig. 3 SP-ICP-MS analysis of AgNPs formed from Ag^+ reduction mediated by nano-BC under different conditions. **a** Concentrations of the newly formed AgNPs in different treatments as a function of time; **b** Dynamics fitting curve of Ag^+ reduction; particle size distributions of AgNPs mediated by **c** nano-WB and **d** nano-PMB, respectively. The concentration of nano-BC was 10 mg/L

by Marković et al. (Markovic et al. 2024). The elemental mapping results also indicated a clear distribution of Ag in the rice leaves and roots, indicating that Ag existed in granular forms or underwent aggregation in the plant tissues (Fig. 4h and S7e). The overall results provide direct evidence that the formed AgNPs in the rhizosphere could be taken up by rice roots and translocated into the leaves.

3.6 Forming mechanism of AgNPs induced by nano-BC

It was reported that the presence of BC in the rhizosphere contributed to the secretion of O_2 from plant root surfaces (Gu et al. 2022). The positive correlation between the concentration of O_2 secreted from root surfaces and the content of formed AgNPs ($R^2 = 0.606$–0.732) in this study suggested that the secreted O_2 might play a crucial role in the Ag^+ reduction (Fig. S9). The relatively high EPR intensity of nano-BC in this study suggested that they contained high contents of PFRs (Fig. S10). These PFRs might activate molecular oxygen to produce ROS (Xiao et al. 2020; Lian et al. 2022). Given the relatively lower reduction potential of biochar (−0.36 to −0.49 V vs. Ag/AgCl (Klupfel et al. 2014; Xin et al. 2019)), the PFRs derived from biochar are thermodynamically favorable for facilitating the reaction of $O_2 \rightarrow O_2^-$ (−0.28 V) (Sun et al. 2019). The cyclic voltammetric results (Fig. S11) also illustrated that nano-BCs exhibited ~ 1.3-fold higher electron donating capacities compared to bulk biochar, revealing its size-dependent redox activity (Gu et al. 2022; Lian and Xing 2024). As a result, we infer that the PFRs in nano-BC were likely to provide lone pair electrons to oxygen molecules secreted from the root surfaces to form O_2^- and participate in the reduction of Ag^+ to AgNPs (Zhang et al. 2024). Previous studies also confirmed that the PFRs in biochar (Zhu et al. 2024) or biochar composite materials (N-BC (Zhu et al. 2024) and Mn-BC (Gao et al. 2022))

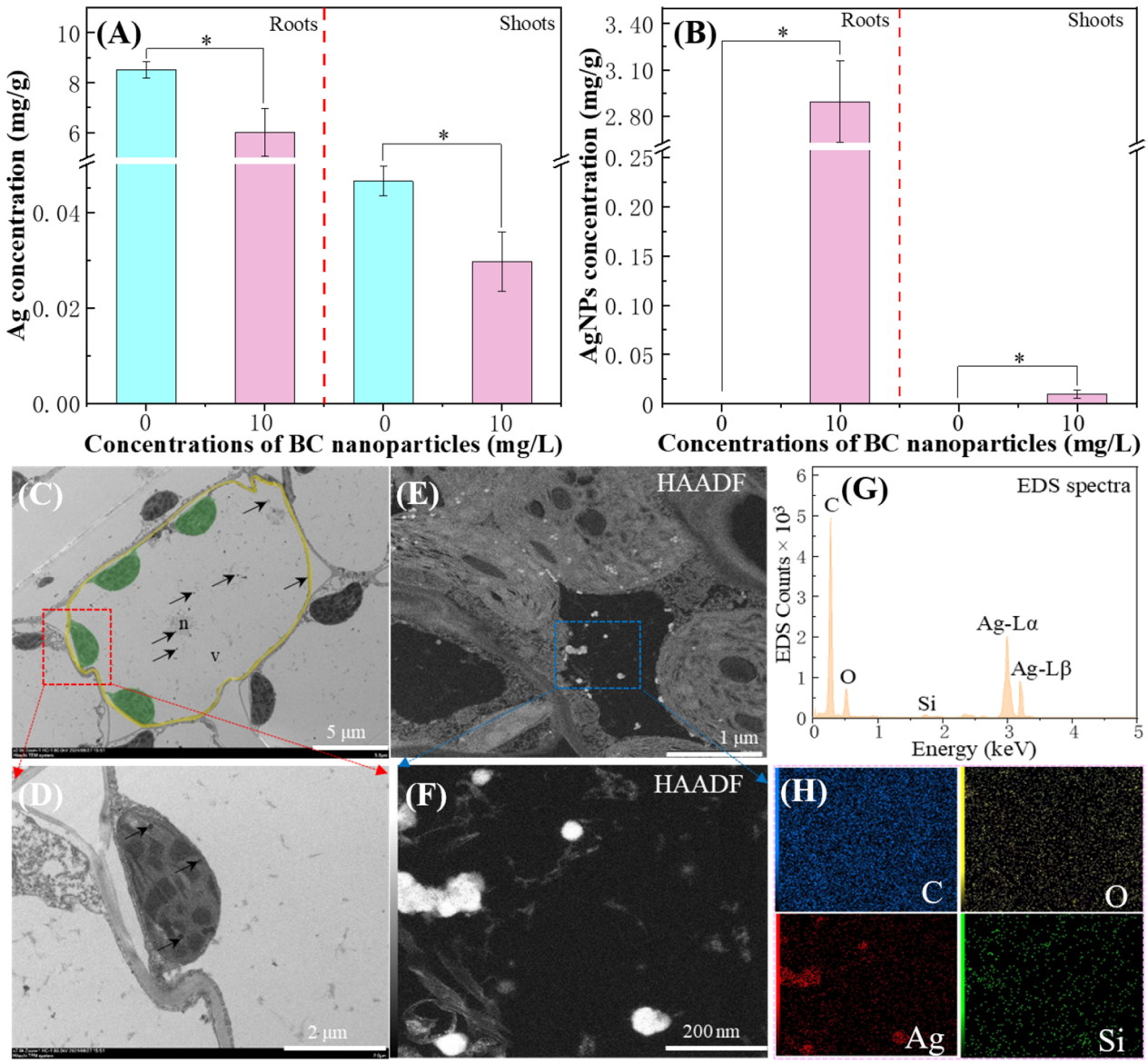

Fig. 4 Concentrations of Ag (**a**) and AgNPs (**b**) in the rice shoots and roots after exposed to Ag^+ and nano-WB in the rhizosphere. (**c**) TEM images and (**e**) STEM images of the rice leaf blade; (**d**) and (**f**) represent the amplification images of zones covered by red and blue dashed squares in (**c**) and (**e**), respectively; (**g**) EDS spectra, and (**h**) EDS elemental mapping. All images were segmented manually: green, chloroplast; yellow, cell wall; n, nucleus; v, vacuole. Arrows point at a few silver clusters. Asterisk (*) represents significant difference ($P < 0.05$) between groups

could transfer electrons to O_2, inducing the formation of O_2^- in the aqueous suspension of biochar. We observed that nano-WB contained 82.63% more PFRs than nano-PMB (Table S4), which might partially explain the higher reduction rate constant (k) of Ag^+ mediated by nano-WB. Consistently, nano-WB exhibited 5 times higher EPR intensity than nano-PMB, which was probably attributed to the higher content of lignin-rich material in the wood biochar (Nitz et al. 2001). The superior PFRs content in nano-WB is structurally attributed to its carbon matrix, characterized by higher oxygen-containing groups (i.e., –OH, C=O, Fig. S1a, b) and sp^2-hybridized carbons (Fig. S1c) (Zhu et al. 2024). Moreover, the higher g-value of nano-WB (2.00402) relative to nano-PMB (2.00398) indicates an enhanced shift of unpaired electrons towards carbon/oxygen in its free radicals (Fig. S10) (Lodygin et al. 2018). Consequently, nano-WB could provide more electron donors for the reduction of Ag^+ and facilitate the formation of AgNPs.

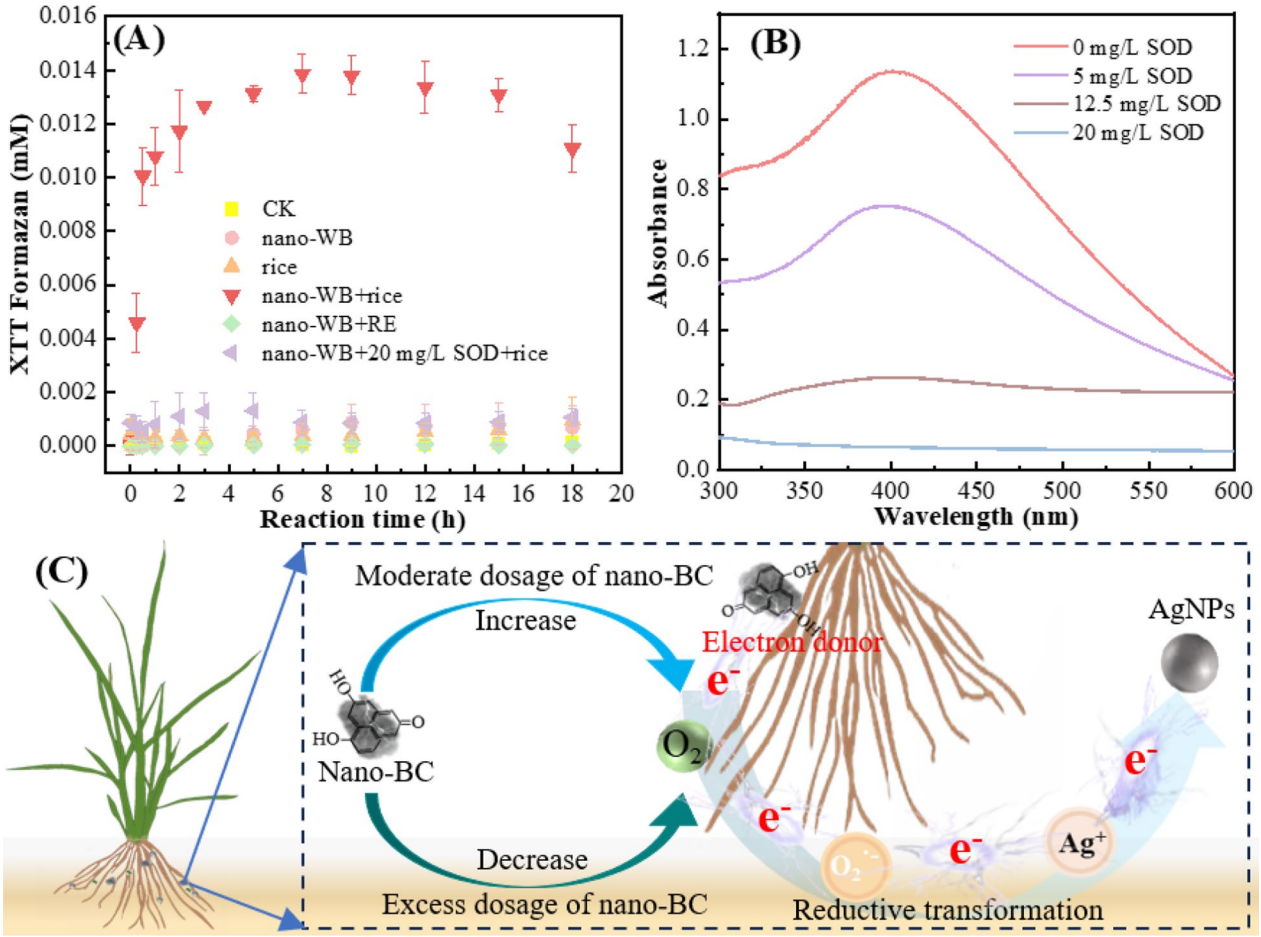

Fig. 5 **a** XTT formazan production as a function of reaction time in the different treatments. The concentration of nano-WB was 10 mg/L. **b** Effects of SOD with different concentrations on the reduction of Ag^+ in the presence of 10 mg/L nano-WB in the rhizosphere. **c** Proposed mechanisms for the reduction of Ag^+ to AgNPs in the presence of nano-BC in the rhizosphere. A moderate concentration of nano-BC facilitated the oxygen secretion at root surfaces, promoting the reduction of Ag^+ to AgNPs. Excessive nano-BC decreased O_2 release by covering root surfaces, thereby inhibiting the reduction of Ag^+

To further demonstrate the critical role of O_2^- in the formation of AgNPs, both probe and quenching experiments were conducted. XTT formazan was only formed in the reaction systems of rice plants + nano-BC, indicative of the generation of O_2^- (Fig. 5a). Consistently, the formation of AgNPs was only observed in the system iv (rice plants + nano-BC + $AgNO_3$) as mentioned above, demonstrating the dominant role of O_2^- in the generation of AgNPs. As expected, the introduction of SOD, a scavenger of O_2^-, significantly reduced the formation of XTT formazan. Interestingly, the UV–Vis characteristic peak of AgNPs decreased gradually as the concentration of SOD increased from 0 to 20 mg/L (Fig. 5b), suggesting the negative effect of SOD on the formation of AgNPs. The result could be explained by the fact that higher concentration of SOD in the rhizosphere displayed stronger ability to scavenge O_2^-, thus resulting in the lower amount of formed AgNPs. These data clearly confirm that O_2^- is the key reductant in the reduction of Ag^+ to AgNPs. Similarly, it was reported that soil organic compounds and dissolved organic compounds played a critical role in the reduction of Ag^+ through promoting the formation of O_2^- (Yin et al. 2012; Huang et al. 2019). The proposed mechanisms for the synergistic effect of nano-BC and secreted O_2 on the reduction of Ag^+ to AgNPs are illustrated in Fig. 5c. Specifically, the higher amount of oxygen functionality (Fig. S1a, Table S2) and larger (O + N)/C ratio (Table S3)) of nano-WB enhance its electron transfer capacity, thereby promoting interactions with Ag^+ via electrostatic attraction and reducing mediation (Yin et al. 2012; Zhu et al. 2024). Conversely, nano-PMB's lower polarity and mineral-rich surface likely impede the reduction of Ag^+ to AgNPs, despite its higher C=C content. Such structure–activity relationships

underscore the importance of tailoring biochar's chemical composition for targeted redox applications.

4 Conclusions

The present study suggests that nano-BC functions not only as a sorbent but also as a robust catalyst in the rhizosphere. The exposure of nano-BC significantly reduced the uptake and accumulation of Ag in the rice plants by forming a barrier on the surfaces of rice roots. Meanwhile, the presence of nano-BC contributed to the reduction of Ag^+ to AgNPs by catalyzing the redox reactions between dioxygen and Ag^+ in the rhizosphere. More importantly, the formed AgNPs could be absorbed by rice roots and translocated to the aboveground tissues.

These observations highlight a hidden pathway through which naturally occurring nanoparticles can enter the food chain, raising concerns about food security and human health. On the other hand, nanomaterials, including AgNPs, hold the potential to enhance plant immunity, contributing to sustainable agriculture. Thus, the catalytic effect of nano-BC in the rhizosphere warrants further investigation to enhance its beneficial functions while mitigating associated risks. Given the ubiquity of nano-BC in terrestrial ecosystems, the impact of nano-BC on elemental cycling especially redox-active elements and their environmental fates also merits more studies.

Supplementary Information

The online version contains supplementary material available at https://doi.org/10.1007/s42773-025-00492-w.

Additional file 1.

Acknowledgements
We greatly appreciate the valuable comments and suggestions from editors and anonymous reviewers.

Author contributions
Shiguo Gu: Writing–original draft, Writing—review and editing, Funding acquisition, Data curation. Binbin Sun: Writing—review and editing, Methodology, Formal analysis. Fei Wang: Writing—review and editing, Methodology. Wei Zhu: Writing—review and editing, Supervision, Investigation. Fei Lian: Writing—review and editing, Methodology, Formal analysis, Funding acquisition. Jie Li: Writing—review and editing, funding acquisition.

Funding
The authors gratefully acknowledge Funding Project for Young Backbone Teachers to Visit and Study in China (JNFX2023061), Chuzhou University Research Initiation Fund Project (2023qd49, 2023qd44), National Natural Science Foundation of China (42207435, 42477263), Natural Science Foundation of Hebei Province (B2023202077, D2022202004), Natural Science Foundation of Tianjin (23JCYBJC00940), China Postdoctoral Science Foundation (2020M680868), and Young Scientists Fund—National Science Foundation of China (42207048).

Data availability
Data will be made available on request.

Declarations

Competing interests
The authors declare that they have no known competing financial interests or personal relationships that could have appeared to influence the work reported in this paper.

Author details
[1]College of Civil and Architecture Engineering, Chuzhou University, Chuzhou 239000, Anhui, China. [2]Institute of Pollution Control and Environmental Health, School of Energy and Environmental Engineering, Hebei University of Technology, Tianjin 300401, China. [3]Agro-Environmental Protection Institute, Ministry of Agriculture and Rural Affairs, Tianjin 300191, China.

Received: 24 February 2025 Revised: 19 June 2025 Accepted: 24 June 2025
Published online: 16 September 2025

References

Adegboyega NF, Sharma VK, Siskova K, Zbořil R, Sohn M, Schultz BJ, Banerjee S (2012) Interactions of aqueous Ag^+ with fulvic acids: mechanisms of silver nanoparticle formation and investigation of stability. Environ Sci Technol 47(2):757–764

Akaighe N, Maccuspie RI, Navarro DA, Aga DS, Banerjee S, Sohn M, Sharma VK (2011) Humic acid-induced silver nanoparticle formation under environmentally relevant conditions. Environ Sci Technol 45:3895–3901

Boldt A, Walter J, Hofbauer F, Stetter K, Aubel I, Bertau M, Jäger CM, Walther T (2023) Cell-free synthesis of silver nanoparticles in spent media of different aspergillus species. Eng Life Sci 23(3):202200052

Cymes BA, Krekeler MPS, Nicholson KN, Grigsby JD (2017) A transmission electron microscopy (TEM) study of silver nanoparticles associated with mine waste from new caledonian nickel deposits: potential origins of silver toxicity in a world heritage site. Environ Earth Sci 76(18):640

Dang F, Wang Q, Cai W, Zhou D, Xing B (2020) Uptake kinetics of silver nanoparticles by plant: relative importance of particles and dissolved ions. Nanotoxicology 14(5):654–666

Dong B, Liu G, Zhou J, Wang J, Jin R (2022) Transformation of silver ions to silver nanoparticles mediated by humic acid under dark conditions at ambient temperature. J Hazard Mater 383:121190

Gao B, Zhu S, Gu J, Liu Y, Yi X, Zhou H (2022) Superoxide radical mediated Mn(III) formation is the key process in the activation of peroxymonosulfate (PMS) by Mn-incorporated bacterial-derived biochar. J Hazard Mater 431:128549

Ge C, Huang D, Wang D, Zhang E, Li M, Zhu F, Zhu C, Chen N, Wu S, Zhou D (2022) Biotic process dominated the uptake and transformation of Ag^+ by shewanella oneidensis MR-1. Environ Sci Technol 56(4):2366–2377

Gu S, Lian F, Han Y, Taherymoosavi S, Mitchell D, Joseph S, Wang Z, Xing B (2022) Nano-biochar modulates the formation of iron plaque through facilitating iron-involved redox reactions on aquatic plant root surfaces. Environ Sci Nano 9(6):1974–1985

Gu S, Zhang W, Wang F, Meng Z, Cheng Y, Geng Z, Lian F (2023) Particle size of biochar significantly regulates the chemical speciation, transformation, and ecotoxicity of cadmium in biochar. Environ Pollut 320:121100

Guo H, Ma C, Thistle L, Huynh M, Yu C, Clasby D, Chefetz B, Polubesova T, White JC, He L, Xing B (2019) Transformation of Ag ions into Ag nanoparticle-loaded AgCl microcubes in the plant root zone. Environ Sc Nano 6(4):1099–1110

Hou WC, Stuart B, Howes R, Zepp RG (2013) Sunlight-driven reduction of silver ions by natural organic matter: formation and transformation of silver nanoparticles. Environ Sci Technol 47(14):7713–7721

Huang YN, Qian TT, Dang F, Yin YG, Li M, Zhou DM (2019) Significant contribution of metastable particulate organic matter to natural formation of silver nanoparticles in soils. Nat Commun 10(1):3775

Huang Y, Dang F, Yin Y, Fang G, Wang Y, Yu G, Zhou D, Xing B (2022) Weathered microplastics induce silver nanoparticle formation. Environ Sci Technol Lett 9(2):179–185

Islam MA, Dada TK, Parvin MI, Vuppaladadiyam AK, Kumar R, Antunes E (2022) Silver ions and silver nanoparticles removal by coffee derived biochar

using a continuous fixed-bed adsorption column. J Water Process Eng 48:102935
Jiang Y, Liu D, Cho M, Lee SS, Zhang F, Biswas P, Fortner JD (2016) In situ photocatalytic synthesis of Ag nanoparticles (nAg) by crumpled graphene oxide composite membranes for filtration and disinfection applications. Environ Sci Technol 50(5):2514–2521
Klupfel L, Keiluweit M, Kleber M, Sander M (2014) Redox properties of plant biomass-derived black carbon (biochar). Environ Sci Technol 48(10):5601–5611
Larue C, Castillo-Michel H, Sobanska S, Cécillon L, Bureau S, Barthès V, Ouerdane L, Carrière M, Sarret G (2014) Foliar exposure of the crop Lactuca sativa to silver nanoparticles: evidence for internalization and changes in Ag speciation. J Hazard Mater 264:98–106
Li Y, Wang X (2012) Root-induced changes in radial oxygen loss, rhizosphere oxygen profile, and nitrification of two rice cultivars in Chinese red soil regions. Plant Soil 365(1–2):115–126
Li LL, Wang XJ, Fu HY, Qu XL, Chen JB, Tao S, Zhu DQ (2020) Dissolved black carbon facilitates photoreduction of Hg (II) to Hg (0) and reduces mercury uptake by lettuce (*Lactuca sativa* L.). Environ Sci Technol 54(18):11137–11145
Li Y, Yu H, Liu L, Yu H (2021) Application of co-pyrolysis biochar for the adsorption and immobilization of heavy metals in contaminated environmental substrates. J Hazard Mater 420:126655
Lian F, Xing B (2024) From bulk to nano: formation, features, and functions of nano-black carbon in biogeochemical processes. Environ Sci Technol 58:15910–15925
Lian F, Gu S, Han Y, Wang Z, Xing B (2022) Novel insights into the impact of nano-biochar on composition and structural transformation of mineral/nano-biochar heteroaggregates in the presence of root exudates. Environ Sci Technol 56(13):9816–9825
Liu L, Tan Z, Gong H, Huang Q (2019) Migration and transformation mechanisms of nutrient elements (N, P, K) within biochar in straw–biochar–soil–plant systems: a review. ACS Sustain Chem Eng 7(1):22–32
Liu Z, Ha S, Liu Y, Wang F, Tao F, Xu B, Yu R, Wang G, Ren F, Li H (2023) Application of Ag-based materials in high-performance lithium metal anode: a review. J Mater Sci Technol 133:165–182
Lodygin ED, Beznosikov VA, Vasilevich R (2018) Paramagnetic properties of humic substances in taiga and tundra soils of the european northeast of russia. Eurasian Soil Sci 51(8):921–928
Mao J, Fang X, Lan Y, Schimmelmann A, Mastalerz M, Xu L, Schmidt-Rohr K (2010) Chemical and nanometer-scale structure of kerogen and its change during thermal maturation investigated by advanced solid-state 13C NMR spectroscopy. Geochim Cosmochim Acta 74:2110–2127
Markovic K, Kesic A, Novakovic M, Grujovic M, Simijonovic D, Avdovic EH, Matic S, Paunovic M, Milutinovic M, Nikodijevic D, Stefanovic O, Markovic Z (2024) Biosynthesis and characterization of silver nanoparticles synthesized using extracts of agrimonia eupatoria L. and in vitro and in vivo studies of potential medicinal applications. Rsc Adv 14(7):4591–4606
Mwanda JA, Cuest A (2021) Reduction of Ag^{+} irreversibly adsorbed on cyanide-modified Pt(111). J Electroanal Chem 896:115039
Nguyen TT, Zhang P, Bi J, Nguyen NH, Dang Y, Xu Z, Wang H, Ninan N, Bright R, Pham T, Nguyen CK, Sabri Y, Nguyen MT, Vongsvivut J, Zhao Y, Vasilev K, Truong VK (2024) Silver-gallium nano-amalgamated particles as a novel, Biocompatible solution for antibacterial coatings. Adv Funct Mater 34(31):2310539
Nitz H, Semke H, Landers R, Mülhaupt R (2001) Reactive extrusion of polycaprolactone compounds containing wood flour and lignin. J Appl Polym Sci 81(8):1972–1984
Peharec Štefanić P, Košpić K, Lyons DM, Jurković L, Balen B, Tkalec M (2021) Phytotoxicity of silver nanoparticles on tobacco plants: evaluation of coating effects on photosynthetic performance and chloroplast ultrastructure. Nanomaterials 11(3):744
Qiu J, Fernandes de Souza M, Robles-Aguilar AA, Ghysels S, Ok YS, Ronsse F, Meers E (2023) Improving biochar properties by co-pyrolysis of pig manure with bio-invasive weed for use as the soil amendment. Chemosphere 312:137229
Qu X, Fu H, Mao J, Ran Y, Zhang D, Zhu D (2016) Chemical and structural properties of dissolved black carbon released from biochars. Carbon 96:759–767
Rahmatpour S, Shirvani M, Mosaddeghi MR, Bazarganipour M (2017) Retention of silver nano-particles and silver ions in calcareous soils: influence of soil properties. J Environ Manage 193:136–145
Riaz M, Roohi M, Arif MS, Hussain Q, Yasmeen T, Shahzad T, Shahzad SM, Muhammad HF, Arif M, Khalid M (2017) Corncob-derived biochar decelerates mineralization of native and added organic matter (AOM) in organic matter depleted alkaline soil. Geoderma 294:19–28
Rogers KR, Henson TE, Navratilova J, Surette M, Hughes MF, Bradham KD, Stefaniak AB, Knepp AK, Bowers L (2020) In vitro intestinal toxicity of commercially available spray disinfectant products advertised to contain colloidal silver. Sci Total Environ 728:138611
Schwertfeger DM, Velicogna JR, Jesmer AH, Saatcioglu S, McShane H, Scroggins RP, Princz JI (2017) Extracting metallic nanoparticles from soils for quantitative analysis: method development using engineered silver nanoparticles and SP-ICP-MS. Anal Chem 89(4):2505–2513
Singh A, Hou WC, Lin TF, Zepp RG (2019) Roles of silver-chloride complexations in sunlight-driven formation of silver nanoparticles. Environ Sci Technol 53(19):11162–11169
Sun T, Levin BD, Guzman JJ, Enders A, Muller DA, Angenent LT, Lehmann J (2017) Rapid electron transfer by the carbon matrix in natural pyrogenic carbon. Nat Commun 8:14873
Sun X, Luo X, Zhang X, Xie J, Jin S, Wang H, Zheng X, Wu X, Xie Y (2019) Enhanced superoxide generation on defective surfaces for selective photooxidation. J Am Chem Soc 141(9):3797–3801
Sun B, Zhang Y, Li R, Wang K, Xiao B, Yang Y, Wang J, Zhu L (2021) New insights into the colloidal stability of graphene oxide in aquatic environment: interplays of photoaging and proteins. Water Res 200:117213
Sun B, Zhang Y, Liu Q, Yan C, Xiao B, Yang J, Liu M, Zhu L (2020) Lateral size dependent colloidal stability of graphene oxide in water: impacts of protein properties and water chemistry. Environ Sci Nano 7(2):634–644
Torrent L, Iglesias M, Marguí E, Hidalgo M, Verdaguer D, Llorens L, Kodre A, Kavčič A, Vogel-Mikuš K (2022) Uptake, translocation and ligand of silver in Lactuca sativa exposed to silver nanoparticles of different size, coatings and concentration. J Hazard Mater 384:121201
Vasileiadis S, Brunetti G, Marzouk E, Wakelin S, Kowalchuk GA, Lombi E, Donner E (2018) Silver toxicity thresholds for multiple soil microbial biomarkers. Environ Sci Technol 52(15):8745–8755
Vrček IV, Žuntar I, Petlevski R, Pavičić I, Dutour Sikirić M, Ćurlin M, Goessler W (2016) Comparison of in vitro toxicity of silver ions and silver nanoparticles on human hepatoma cells. Environ Toxicol 31(6):679–692
Wang X, Tam NF, He H, Ye Z (2015) The role of root anatomy, organic acids and iron plaque on mercury accumulation in rice. Plant Soil 394:301–313
Xiang QQ, Gao Y, Li QQ, Ling J, Chen LQ (2020) Proteomic profiling reveals the differential toxic responses of gills of common carp exposed to nanosilver and silver nitrate. J Hazard Mater 394:122562
Xiao Y, Lyu H, Tang J, Wang K, Sun H (2020) Effects of ball milling on the photochemistry of biochar: Enrofloxacin degradation and possible mechanisms. Chem Eng J 384:123311
Xin D, Xian M, Chiu PC (2019) New methods for assessing electron storage capacity and redox reversibility of biochar. Chemosphere 215:827–834
Xu CL, Xue YJ, Qi YZ, Wang XC (2016) Quantities and fluxes of dissolved and particulate black carbon in the changjiang and huanghe rivers, China. Estuaries Coasts 39:1617–1625
Yang P, Peng J, Chu Z, Jiang D, Jin W (2017) Facile synthesis of prussian blue nanocubes/silver nanowires network as a water-based ink for the direct screen-printed flexible biosensor chips. Biosens Bioelectron 92:709–717
Yao Y, Gao B, Chen J, Yang L (2013) Engineered biochar reclaiming phosphate from aqueous solutions: mechanisms and potential application as a slow-release fertilizer. Environ Sci Technol 47(15):8700–8708
Yin Y, Liu J, Jiang G (2012) Sunlight-induced reduction of ionic Ag and Au to metallic nanoparticles by dissolved organic matter. ACS Nano 6(9):7910–7919
Yu C, Zhu X, Mohamed A, Dai K, Cai P, Liu S, Huang Q, Xing B (2023) Enhanced Cr (VI) bioreduction by biochar: insight into the persistent free radicals mediated extracellular electron transfer. J Hazard Mater 442:129927
Yue L, Lian F, Han Y, Bao Q, Wang Z, Xing B (2019) The effect of biochar nanoparticles on rice plant growth and the uptake of heavy metals: implications for agronomic benefits and potential risk. Sci Total Environ 656:9–18
Zhang X, Yang CW, Yu HQ, Sheng GP (2016) Light-induced reduction of silver ions to silver nanoparticles in aquatic environments by microbial extracellular polymeric substances (EPS). Water Res 106:242–248

Zhang X, Wells M, Niazi NK, Bolan N, Shaheen S, Hou D, Gao B, Wang H, Rinklebe J, Wang Z (2022) Nanobiochar-rhizosphere interactions: implications for the remediation of heavy-metal contaminated soils. Environ Pollut 299:118810

Zhang P, Tang X, Qin N, Shuai Y, Wang J, Wang H, Ouyang Z, Jia H (2024) Advanced understanding of the natural forces accelerating aging and release of black microplastics (tire wear particles) based on mechanism and toxicity analysis. Water Res 266:122409

Zhao X, Zhou L, Xu X, Ai C, Zhao P, Yan L, Jiang C, Shi J (2021) Recovery of Ag^{+} by cyclic lipopeptide iturin A and corresponding chain peptide: reaction mechanisms, kinetics, toxicity reduction, and applications. Sci Total Environ 763:142988

Zhu K, Ma S, Chen N, Dai Y, Wang T, Guo X, Jia H (2024) Robust reactive oxygen species production in interfacial reaction between organic acids and biochar: the combined effect of electron acceptance and electron conduction. J Hazard Mater 464:132960